VSP

Journal of Adhesion Science and Technology 22 (2008) 217–229

Journal of ADHESION SCIENCE and TECHNOLOGY
www.brill.nl/jast

An Electrowetting Model for Rough Surfaces Under Low Voltage

Wei Dai and Ya-Pu Zhao *

State Key Laboratory of Nonlinear Mechanics (LNM), Institute of Mechanics, Chinese Academy of Sciences, Beijing 100080, China

Received in final form 30 December 2007

Abstract

Electrowetting is one of the most effective methods to enhance wettability. A significant change of contact angle for the liquid droplet can result from the surface microstructures and the external electric field, without altering the chemical composition of the system. During the electrowetting process on a rough surface, the droplet exhibits a sharp transition from the Cassie–Baxter to the Wenzel regime at a low critical voltage. In this paper, a theoretical model for electrowetting is put forth to describe the dynamic electrical control of the wetting behavior at the low voltage, considering the surface topography. The theoretical results are found to be in good agreement with the existing experimental results.

Keywords

Electrowetting, contact angle, rough surface, Young's equation, Lippmann–Young equation, Wenzel's equation, Cassie–Baxter equation

1. Introduction

The manipulation of the microfluidics is one of the most important applications in microelectromechanical systems (MEMS), such as the lab-on-a-chip and biomedical microdevice systems [1–4]. The classical effect of electrowetting on dielectric (EWOD) [5, 6] is to make a droplet flatten and spread by applying voltage between the electrodes in the droplet and under the dielectric coating. As the electrical control of the microfluidic motion is significantly more promising for microdevices and easy to manipulate, electrowetting has attracted much research interest [7–13].

When a liquid droplet is placed on a solid surface, it remains as a drop exhibiting a specific contact angle between the liquid and solid phase or spreads across the surface to form a wetting film. In 1805 Young described the contact angle θ_0 for

* To whom correspondence should be addressed. Tel.: (86-10) 8254-3932; Fax: (86-10) 8254-3977; e-mail: yzhao@imech.ac.cn

 DOI:10.1163/156856108X306966

a smooth surface at the three-phase contact line [14], deriving it from the force equilibrium in the horizontal direction by the interfacial tensions at the solid–vapor (γ_{sv}), liquid–vapor (γ_{lv}) and solid–liquid (γ_{sl}) interfaces:

$$\cos\theta_0 = \frac{\gamma_{sv} - \gamma_{sl}}{\gamma_{lv}}, \tag{1}$$

which is generally called Young's equation. The origin of surface tension γ can be explained at the molecular level [15].

The topography patterns on surfaces play a crucial effect in wetting in natural systems [16, 17], such as the configuration of lotus leaves. The roughness effect is classically described by Wenzel's law [18] as:

$$\cos\theta = R\cos\theta_0, \tag{2}$$

where θ is the contact angle on rough surfaces and R is the roughness factor, given as the ratio of actual to apparent (geometric) solid–liquid contact areas:

$$R = \frac{A_{sl(actual)}}{A_{sl(apparent)}}. \tag{3}$$

For the case in which the surface is heterogeneous with fractions of open air [19, 20], an alternative model for the composite surface was developed by Cassie and Baxter [21]. If f_1 is the total area of solid–liquid interface and f_2 the total area of liquid–air interface in a plane geometrical area of unity parallel to the rough surface ($f_1 + f_2 = 1$), then the contact angle θ_c for the composite surface is expressed by

$$\cos\theta_c = f_1\cos\theta_0 - f_2. \tag{4}$$

If the contact angle is large and the surface is sufficiently rough, the apparent contact angle from equation (4) becomes [22]:

$$\cos\theta_c = Rf_1\cos\theta_0 - f_2. \tag{5}$$

These models are widely used in the analysis and preparation of the solid–liquid–air composite surfaces, especially for the superhydrophobic surfaces.

Electrowetting is the phenomenon of enhancing the wettability of a solid surface by applying an external voltage across the solid–liquid interface [22]. Lippmann was the first to conclude that the electrocapillary force at the interface could be modified by external static charges [24]. The Lippmann equation was extended to the well-known Lippmann–Young equation [12], which is currently adopted as the basis for almost all discussions regarding electrowetting. Because of the miniaturization tendency in MEMS, the large surface area-to-volume ratio of the microdevices causes serious surface effects in the electrowetting. The results of electrowetting experiments on rough surfaces show that the cosine of the apparent contact angle is proportional to the square of the increasing voltage. However, there is always a critical voltage which is usually low in these experiments. The rate of change of the cosine of the contact angle before this critical voltage is smaller

than after. Besides, the Lippmann–Young equation cannot describe the contact angle variation on rough surfaces. The Wenzel and Lippmann equations have been combined to describe the contact angle change after the critical voltage on rough surfaces [25]. As far as we know, there is no theoretical model to describe the electrowetting phenomenon on a rough surface before this critical voltage. In this paper, we attempt to establish an electrowetting model to describe the electrowetting behavior at a low voltage, including the influence of the surface microstructure. Our work is compared with the existing experimental results in the published literature. For the nomenclature used in this study, the reader is referred to Appendix A.

2. Theory

The most popular experimental configuration of electrowetting is shown in Fig. 1. The shape of droplet without applied voltage is shown in Fig. 1 by the dashed line, while the shape with applied voltage is shown by the solid line. EWOD enables manipulation of liquid droplets by electrically controlling surface wettability, manifested by the contact angle between the liquid and dielectric coating. If the sessile droplet is large enough, it will tend to flatten under the influence of gravity. We neglect the gravity in this paper as the droplet diameter is much smaller than the capillary length [26], which is 2.7 mm for water. At this length scale, the surface tension is at the dominant status to the shape of the droplet. In the absence of external electric fields, the behavior of droplet is determined by surface tension alone.

2.1. Electrowetting on Smooth Surfaces

In 1875, through the study on the interface between the electrolyte solution and hydrargyrum (also known as mercury), Lippmann [24] put forward the equation

$$\sigma_{\mathrm{sl}} = -\left(\frac{\partial \gamma_{\mathrm{sl}}}{\partial U}\right)_{\mu,P,T}, \tag{6}$$

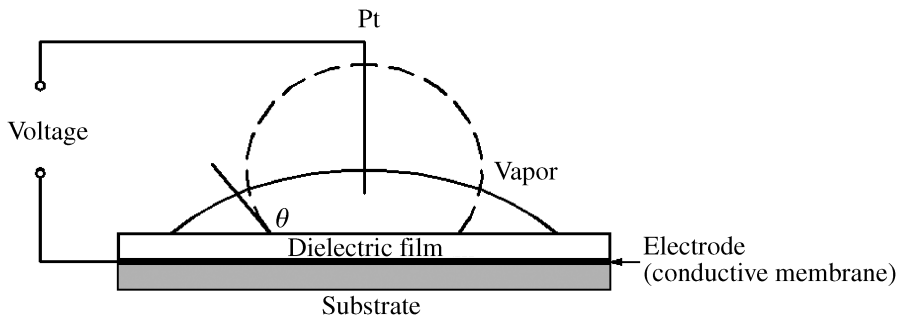

Figure 1. Electrowetting behaviour of a conductive liquid on a dielectric film. The external voltage, which causes the droplet to spread, is applied between a thin Pt wine electrode and a well conductive membrane on the glass.

where σ_{sl} is the surface charge density at the solid–liquid interface and U is the voltage difference applied across the interface. Equation (6), which is called the Lippmann equation, describes the relation between solid–liquid surface tension, voltage and surface charge at a constant temperature T, pressure P and chemical potential μ. Under special conditions, Lippmann's equation can be deduced from the Gibbs adsorption formula and the Nernst formula [27]. When the Lippmann equation is applied in the case of EWOD, the dielectric layer is considered as part of the effective solid–liquid interface [13]. Then integrating equation (6), assuming the capacitance is independent of the voltage, yields

$$\gamma_{sl} = \gamma_{sl0} - \frac{1}{2} C U^2, \tag{7}$$

where γ_{sl0} is the surface tension at the point of zero charge, and for a simple planar surface the capacitance per unit area is $C = \varepsilon\varepsilon_0/d$, where d is the thickness of the insulator film in the electrowetting, and ε and ε_0 are the dielectric constants of the insulator film and vacuum, respectively. When equation (7) is substituted into the classic Young's equation, the famous Lippmann–Young equation, which predicts the contact angle θ_e for electrowetting, is derived:

$$\cos\theta_e = \cos\theta_0 + \eta, \tag{8}$$

where θ_0 is the contact angle without any voltage and $\eta = \varepsilon\varepsilon_0 U^2/(2d\gamma_{lv})$ is a dimensionless electrowetting number, which represents the ratio between electrostatic energy per unit area and the surface tension [12]. Equation (8) is used only for a smooth surface. It must be mentioned that as the electric double layer is formed at a metal–electrolyte interface, the electric field at a metal–electrolyte interface can induce a change in surface tension [6]. However, electrowetting on conductive surfaces has the limitation of the electron transfer from the electrode to redox-active species in the liquid, so the EWOD for general applications has been developed rapidly in the recent years. As the electrolyte solution is treated as a perfect conductor, the property of the dielectric layer mainly determines the storage of the electrostatic energy [13]. In this paper, our attention is focused on the EWOD.

2.2. Extended Electrowetting Equation

In an electrowetting experiment, one can achieve from superhydrophobicity to almost complete wetting for liquids on microstructured surfaces [28]. Another important phenomenon is also reported, i.e., the apparent contact angle will reduce suddenly at a critical voltage, because the liquid penetrates into the grooves [25, 28]. The rate of change of the cosine of the contact angle is different before or after this critical voltage. The apparent contact angle change after the critical voltage can be predicted by the combined expression of Wenzel and Lippmann equations.

On the basis of the macroscopic balance condition of the horizontal force components at the three-phase contact line, the conventional electrowetting equation is derived. The latest studies about how electrostatic fields alter the contact angle in

electrowetting show that in the vicinity of the three-phase contact line, the electric force *via* the Maxwell stress is balanced by the Laplace pressure, i.e.,

$$\Pi_{\mathrm{el}}(\bar{r}) = 2\gamma_{\mathrm{lv}}\kappa(\bar{r}), \tag{9}$$

where $\Pi_{\mathrm{el}}(\bar{r}) = \frac{\varepsilon_0}{2}\bar{E}(\bar{r})^2$ is the Maxwell stress, $\bar{E}(\bar{r})$ is the local electric field, $P_{\mathrm{L}} = 2\gamma_{\mathrm{lv}}\kappa(\bar{r})$ is the Laplace pressure, $\kappa(\bar{r}) = (1/r_1 + 1/r_2)/2$ is the mean curvature, and r_1 and r_2 are the two principal radii of curvature of the surface. Its effect is just to locate the contact angle around the contact line and its influence distance from the contact line only approximately equals the thickness of the dielectric layer [8, 29, 30]. As the contact angle studied in this paper is at the macroscopic scale, the approach to minimize the free energy of the system is also used to extend the electrowetting equation to rough surfaces.

Here the way Cassie and Baxter treated a composite surface is used to extend the classical electrowetting equations to microstructured surfaces. For simplicity, the optimized rough surface with hemispherically topped cylindrical asperities for superhydrophobicity [31] is shown as an example in our model (Fig. 2). The total system energy including both the surface and electrostatic energies becomes

$$E_{\mathrm{tot}} = \gamma_{\mathrm{lv}}A_{\mathrm{lv}} + (-\gamma_{\mathrm{sv}}A_{\mathrm{sl}} + \gamma_{\mathrm{sl}}A_{\mathrm{sl}}) - E_{\mathrm{e}}A_{\mathrm{sl}}, \tag{10}$$

where E_{e} is the electrostatic energy per unit area. Here the contact area is divided into two parts at the composite interface. One part is for the solid–liquid interface, and the other is for the liquid–air interface:

$$\begin{aligned} E_{\mathrm{tot}} = {} & \gamma_{\mathrm{lv}}A_{\mathrm{lv}} + [(-\gamma_{\mathrm{sv1}}A_{\mathrm{sl1}} + \gamma_{\mathrm{sl1}}A_{\mathrm{sl1}}) - E_{\mathrm{e}}A_{\mathrm{sl1}}] \\ & + (-\gamma_{\mathrm{sv2}}A_{\mathrm{sl2}} + \gamma_{\mathrm{sl2}}A_{\mathrm{sl2}}). \end{aligned} \tag{11}$$

The variation of the liquid–vapor interfacial tension is very small, about 2% when an electric field with a magnitude of 10^6 V/m is applied [32], and can be neglected.

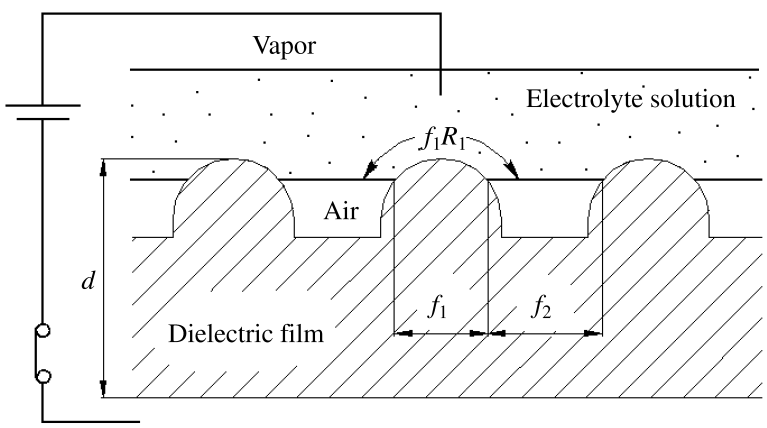

Figure 2. Electrowetting on an optimized rough surface with hemispherically topped cylindrical asperities. The air remains in the grooves, and the roughness in the solid–liquid contact area is R_1.

Thus, the electric energy effect is mainly on the solid–liquid interface. Because γ_{sv2} is zero and γ_{sl2} is simply γ_{lv} at the part of the grooves with the air [22], equation (11) becomes

$$E_{tot} = \gamma_{lv} A_{lv} + [(-\gamma_{sv1} A_{sl1} + \gamma_{sl1} A_{sl1}) - E_e A_{sl1}] + \gamma_{lv} A_{sl2}. \tag{12}$$

At the equilibrium $dE_{tot} = 0$, and combining the geometrical consideration of the contact angle, we obtain

$$\cos\theta_c = \frac{dA_{lv}}{dA_{sl}} = \frac{dA_{sl_1}}{dA_{sl}}\left(\frac{\gamma_{sv1} - \gamma_{sl1}}{\gamma_{lv}} + \frac{E_e}{\gamma_{lv}}\right) - \frac{dA_{sl_2}}{dA_{sl}}, \tag{13}$$

which is the same as the Cassie–Baxter equation, taking $f_1 = dA_{sl1}/dA_{sl}$, $f_2 = dA_{sl2}/dA_{sl}$ [21]. Substituting the Young equation into equation (13), it becomes

$$\cos\theta_c = f_1\left(\cos\theta_0 + \frac{E_e}{\gamma_{lv}}\right) - f_2. \tag{14}$$

The solid–liquid contact area is generally not smooth, therefore, the roughness factor R_1 of the solid–liquid part [22] is added in equation (14), which yields

$$\cos\theta_c = R_1 f_1\left(\cos\theta_0 + \frac{E_e}{\gamma_{lv}}\right) - f_2. \tag{15}$$

Though the top of the asperities is not always smooth, for simplicity and without loss of generality, E_e approximates to the value of a plane surface here. The electric effect on the asperity having a small rough top is discussed in Appendix B. The value of E_e for an isotropic planar film is

$$E_e = \int_0^d \frac{1}{2} E D \, dz, \tag{16}$$

where z is the coordinate perpendicular to the film surface, E is the electric field and D is the electric displacement with $D = \varepsilon\varepsilon_0 E$. Therefore, the electrostatic energy per unit area at the interface is

$$E_e = \frac{\varepsilon\varepsilon_0 U^2}{2d}, \tag{17}$$

and now equation (15) can be written as

$$\cos\theta_c = R_1 f_1\left(\cos\theta_0 + \frac{1}{2}\frac{\varepsilon\varepsilon_0 U^2}{d\gamma_{lv}}\right) - f_2. \tag{18}$$

Then, by substituting the dimensionless electrowetting number η in equation (18), we obtain

$$\cos\theta_c = R_1 f_1(\cos\theta_0 + \eta) - f_2. \tag{19}$$

Equation (19) is the extended Lippmann–Young equation based on the Cassie–Baxter model, which can be applied to the electrowetting phenomenon on a rough surface. When the external electric field effect is removed, $\eta = 0$, and equation (19)

reduces to the Cassie–Baxter equation with sufficient roughness (equation (5)). If the surface is just heterogeneous, then R_1 equals unity, and equation (19) reduces to equation (4). In the case that the surface is rough but without trapped air, f_2 is zero, and equation (19) reduces to the Wenzel equation. Similarly, when the surface is smooth, the equation reduces to the Lippmann–Young equation (8).

As the potential difference between the two phases is increased, at some critical voltage the liquid wicks into the grooves of the composite surface. Consequently, this extended equation is suitable under this critical voltage which is generally low, as the droplet is still levitated on the asperities of the surface.

3. Results and Discussion

Figure 3b presents the electrowetting experimental results from Herbertson et al. [25] on a micro-patterned layer of SU-8 photoresist with an amorphous Teflon® coating. The electrolyte solution is deionized water with 0.01 M KCl. The voltage is applied from 0 V to 130 V. In this experiment, it is observed that before 45 V the contact angle changes only little, but after this voltage the contact angle changes appreciably. The size of the microstructure at the surface is given in Ref. [25]. The complete structure consists of cylindrical pillars 7.0 ± 0.5 μm in diameter with a center-to-center separation of 15 μm and a thickness of 6.5 ± 1.3 μm and on a base layer with a thickness of approximately 8.5 μm (Fig. 3a). The water contact angle on a plane Teflon® AF film is 113.9°. The results in Fig. 3b show the change in contact angle in the voltage cycle from 0 up to 130 V and back to 0 V in the experiment. The data shown in the bottom plot represent the contact angle change with increasing voltage, and the data in the top plot represent the contact angle change under decreasing voltage. There is a critical voltage, where there is a change in the slope of the data in the electrowetting process under increasing voltage. The wetting behavior transitions from the Cassie–Baxter to Wenzel regime at this voltage. We compare the theoretical values from the extended electrowetting equation (equation (19)) to these experimental results [25] before the critical voltage. As the liquid does not wick into the grooves in the Cassie–Baxter model, the effect of small bridges among the cylinders in the electrowetting experiment can be neglected before the critical voltage.

The two area fractions are $f_1 = 7.0\ \mu\text{m}/15\ \mu\text{m} = 0.467$, $f_2 = 1 - f_1 = 0.533$ from these experiments [25] and, as the top of SU-8 microstructure is flat, the roughness of the solid–liquid contact area R_1 is equal to the roughness of the top asperity (R_{top}) here, which can be derived from the Cassie–Baxter equation (equation (5)), as $\cos 144.3° = R_1 f_1 \cos 113.9° - f_2$ in Ref. [25]. It is calculated that $R_1 = R_{\text{top}} = 1.474$. In Fig. 4, the experimental results [25] in the Wenzel regime (45–130 V) are fitted by a line, as the contact angle under these voltages can be described by the combined Wenzel and Lippmann equations [25]:

$$\cos\theta_{\text{e}} = R\left(\cos\theta_0 + \frac{1}{2}\frac{\varepsilon\varepsilon_0 U^2}{d\gamma_{\text{lv}}}\right). \tag{20}$$

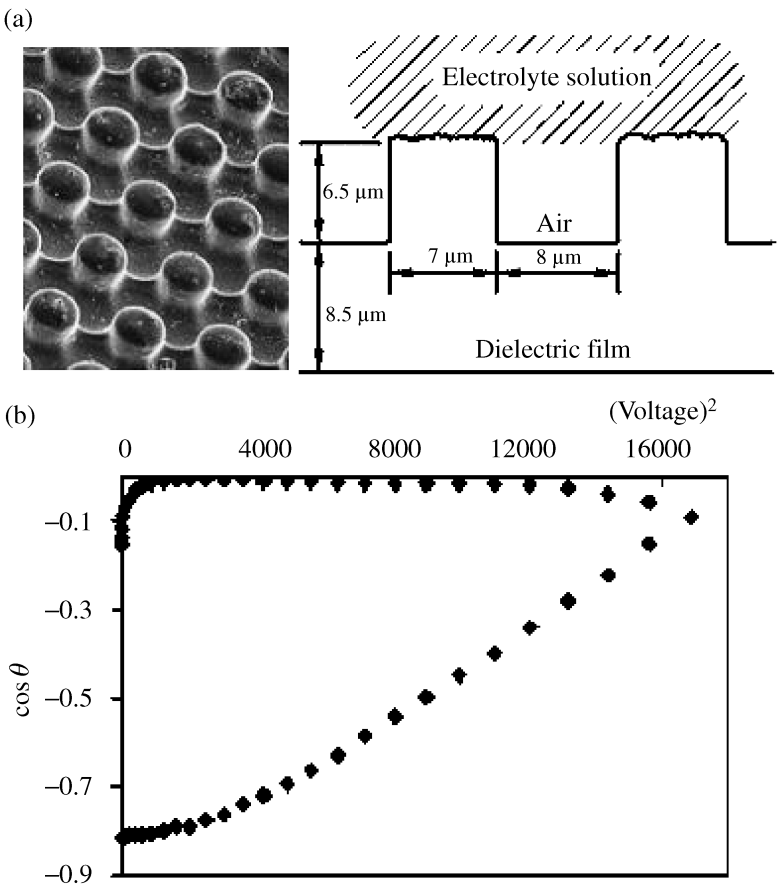

Figure 3. (a) SEM image of the pillars on the dielectric film [25] and the schematic of the microstructures. (b) Change of contact angle in the voltage cycle from 0 up to 130 V and back to 0 V in the experiment [25].

Equation (20) is applied to the electrowetting after the critical voltage. The cosine of the contact angle is directly proportional to the squared voltage, thus the slope can be obtained as $R\varepsilon\varepsilon_0/2d\gamma_{\mathrm{lv}} = 4.70 \times 10^{-5}$, and the intercept is -0.909. As the contact angle on the plane surface is 113.9°, the roughness R of the whole surface can be derived as 2.24 via the Wenzel equation (equation (2)), from $-0.909 = R\cos 113.9°$. Thus, we can obtain the coefficient before the squared voltage in the dimensionless electrowetting number η as:

$$\frac{\varepsilon\varepsilon_0}{2d\gamma_{\mathrm{lv}}} = 2.10 \times 10^{-5}. \tag{21}$$

Substituting all these parameters into equation (18), the theoretical values are shown in Fig. 5 and are compared with the experimental results from 0 V to 45 V [25]. In Fig. 5, the straight line represents the predicted values obtained from the extended electrowetting equation, and the small square boxes are taken from the experimental

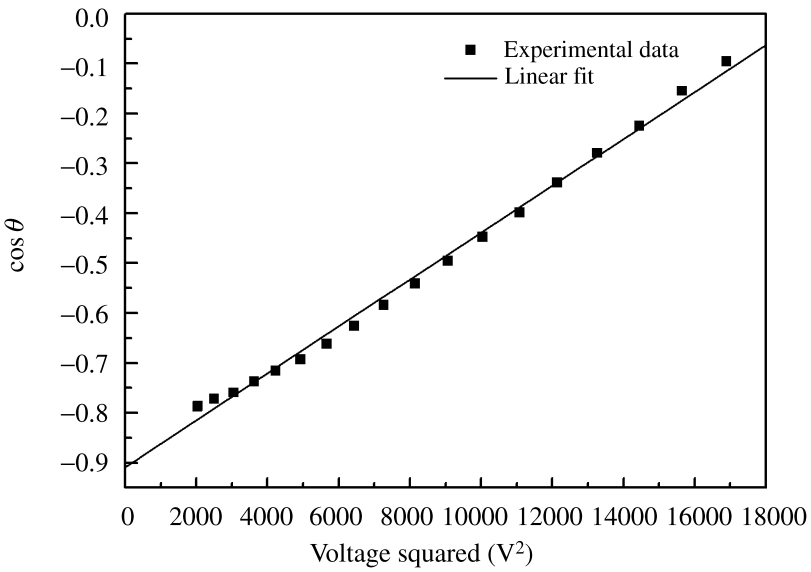

Figure 4. The linear fit of the experimental results [25] in the Wenzel regime.

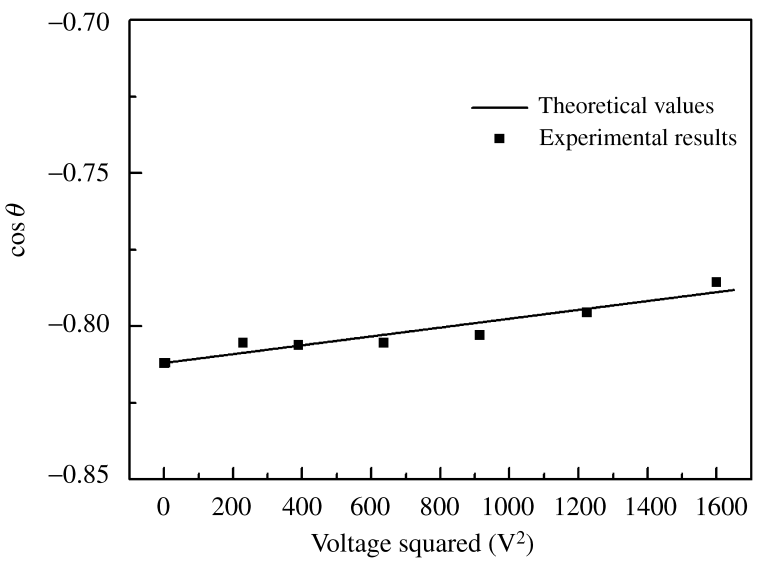

Figure 5. The straight line represents the theoretical values from the extended electrowetting equation; the small square boxes are the experimental results [25] in the Cassie–Baxter regime.

results in Fig. 3b before 45 V. The theoretical values almost predict the experimental results in Ref. [25].

It should be noted that the comparison between the theoretical values and the experimental data mentioned above is based on a single kind of periodic microstructure surface. As far as the authors, are aware there are no other suitable experimental

data to validate our model. More experimental electrowetting data on rough surfaces are expected to validate the extended electrowetting equation (19) derived in this paper.

4. Conclusion

In this work, an extended electrowetting equation is derived from the classic wetting equations for liquids on rough surfaces. This equation can predict the contact angle change under the electric field before the transition from the Cassie–Baxter to Wenzel regime. The predicted values from the extended electrowetting equation agree well with the existing experimental results.

Acknowledgements

This work was supported by the National Basic Research Program of China (973 Program, Grant No. 2007CB310500) and National Natural Science Foundation of China (NSFC, Grant No. 10772180). Helpful discussions with Prof. F. Mugele, Dr. M. I. Newton and Li-Ya Guo are gratefully acknowledged.

References

1. M. G. Pollack, A. D. Shenderov and R. B. Fair, *Lab on a Chip* **2**, 96–101 (2002).
2. S. K. Cho, H. J. Moon and C.-J. Kim, *J. Microelectromech. Syst.* **12**, 70–80 (2003).
3. O. D. Velev, B. G. Prevo and K. H. Bhatt, *Nature* **426**, 515–516 (2003).
4. Y.-H. Chang, G.-B. Lee, F.-C. Huang, Y.-Y. Chen and J.-L. Lin, *Biomed. Microdevices* **8**, 215–225 (2006).
5. H. J. J. Verheijen and M. W. J. Prins, *Langmuir* **15**, 6616–6620 (1999).
6. H. Moon, S. K. Cho, R. L. Garrell and C.-J. Kim, *J. Appl. Phys.* **92**, 4080–4087 (2002).
7. C. Quilliet and B. Berge, *Curr. Opin. Colloid Interface Sci.* **6**, 34–39 (2001).
8. J. Buehrle, S. Herminghaus and F. Mugele, *Phys. Rev. Lett.* **91**, 086101 (2003).
9. P. S. Swain and R. Lipowsky, *Langmuir* **14**, 6772–6780 (1998).
10. T. B. Jones, *J. Micromech. Microeng.* **15**, 1184–1187 (2005).
11. A. Quinn, R. Sedev and J. Ralston, *J. Phys. Chem. B* **109**, 6268–6275 (2005).
12. F. Mugele, A. Klingner, J. Buehrle, D. Steinhauser and S. Herminghaus, *J. Phys.: Condens. Matter* **17**, S559–S576 (2005).
13. F. Mugele and J.-C. Baret, *J. Phys.: Condens. Matter* **17**, R705–R774 (2005).
14. T. Young, *Philos. Trans. Roy. Soc. London* **95**, 65–87 (1805).
15. P.-G. de Gennes, F. Brochard-Wyart and D. Quéré, *Capillarity and Wetting Phenomena: Drops, Bubbles, Pearls, Waves.* Springer, New York, NY (2004).
16. C. Neinhuis and W. Barthlott, *Ann. Botany* **79**, 667–677 (1997).
17. G. Palasantzas and J. T. M. de Hosson, *Acta Mater.* **49**, 3533–3538 (2001).
18. R. N. Wenzel, *Ind. Eng. Chem.* **28**, 988–994 (1936).
19. S. L. Ren, S. R. Yang and Y. P. Zhao, *Acta Mech. Sin.* **20**, 159–164 (2004).
20. S. L. Ren, S. R. Yang, Y. P. Zhao, T. X. Yu and X. D. Xiao, *Surface Sci.* **546**, 64–74 (2003).
21. A. B. D. Cassie and S. Baxter, *Trans. Faraday Soc.* **40**, 546–551 (1944).
22. A. W. Adamson, *Physical Chemistry of Surfaces*, 5th edn. Wiley-Interscience, New York, NY (1990).

23. W. J. J. Welters and L. G. J. Fokkink, *Langmuir* **14**, 1535–1538 (1998).
24. G. Lippmann, *Ann. Chim. Phys.* **5**, 494–548 (1875).
25. D. L. Herbertson, C. R. Evans, N. J. Shirtcliffe, G. McHale and M. I. Newton, *Sensors Actuators A* **130**, 189–193 (2006).
26. D. Langbein, *Capillary Surfaces*: *Shape-Stability-Dynamics, in Particular under Weightlessness*. Springer, Berlin (2002).
27. L. I. Antropov, *Theoretical Electrochemistry.* Mir Publishers, Moscow (1977).
28. T. N. Krupenkin, J. A. Taylor, T. M. Schneider and S. Yang, *Langmuir* **20**, 3824–3827 (2004).
29. M. Bienia, M. Vallade, C. Quilliet and F. Mugele, *Europhys. Lett.* **74**, 103–109 (2006).
30. K. H. Kang, *Langmuir* **18**, 10318–10322 (2002).
31. M. Nosonovsky and B. Bhushan, *Microsyst. Technol.* **11**, 535–549 (2005).
32. A. Bateni, S. S. Susnar, A. Amirfazli and A. W. Neumann, *Langmuir* **20**, 7589–7597 (2004).

Appendix A: Nomenclature

A, A_{sl}, A_{lv}, A_{sv}	Surface area
C	Capacitance
d	Height of the insulator film
d'	Height of the bulge at the asperity top
D	Electric displacement
E	Electric field
E_{tot}	Total energy of the system
E_e	Electrostatic energy per unit area
f_1, f_2	Fraction of the surface
l	Bottom length of the asperity profile
l'	Top length of the asperity profile
P	Pressure
P_L	Laplace pressure
R, R_1, R_{top}	Roughness factor
$r_{1,}r_2$	Principal radii of curvature of the surface
T	Temperature
U	Voltage
γ, γ_{sv}, γ_{lv}, γ_{sl}	Surface or interfacial tension
ε_0	Vacuum permittivity
ε	Dielectric constant of the insulator film
η	Electrowetting number
κ	Mean curvature of the liquid–vapor interface
μ	Chemical potential
Π_{el}	Maxwell stress
$\theta, \theta_0, \theta_c, \theta_e$	Contact angle
σ	Surface charge density

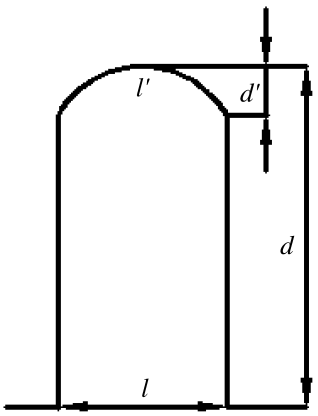

Figure B1. The sketch of the asperity in the electric field. l and l' are the lengths of the profiles of asperities at the bottom and top, respectively. The height of the bulge at the top of the asperity is d'.

Appendix B: Electrostatic Energy per Unit Area on an Asperity With a Small Rough Top

In the electrostatic field, the number of electric field lines in an asperity is constant. For the small difference in the surface areas at the asperity's top and bottom, the electric field is slightly smaller at the top than at the bottom. Let the electric field at the bottom be E_0, l and l' be the lengths of the profiles of asperities at the bottom and top, respectively (the sketch of the asperity is shown in Fig. B1). Thus, the electric field at top is $E_0 l/l'$. The thickness of the dielectric film is d, and let the height of the bulge at the top of the asperity be d'. The electric field is uniform except at the raised part at top. It is assumed that the electric field decreases linearly as:

$$E = E_0 \frac{l}{l'} + kd', \tag{B1}$$

where

$$k = \frac{E_0}{d'}\left(1 - \frac{l}{l'}\right). \tag{B2}$$

Thus the electrostatic energy per unit area is

$$\begin{aligned} E_\mathrm{e} &= \frac{1}{2}\varepsilon\varepsilon_0 \int_0^{d'} \left(E_0 \frac{l}{l'} + kd'\right)^2 \mathrm{d}z + \frac{1}{2}\varepsilon\varepsilon_0 \int_0^{d-d'} E_0 \,\mathrm{d}z \\ &= \frac{1}{2}\varepsilon\varepsilon_0 E_0^2 \left(\frac{1}{3}\frac{l}{l'}d' - \frac{2}{3}d' + \frac{1}{3}\frac{l^2}{l'^2}d' + d\right). \end{aligned} \tag{B3}$$

At the same time the voltage is expressed as

$$U = \int_0^{d'} \left(E_0 \frac{l}{l'} + kd'\right) \mathrm{d}z + E_0(d - d') = E_0 \left(\frac{1}{2}\frac{l}{l'}d' - \frac{1}{2}d' + d\right). \tag{B4}$$

Therefore, the electrostatic energy per unit area becomes

$$E_e = \frac{1}{2}\frac{\varepsilon\varepsilon_0}{d}\frac{1+(1/3)(l/l')(d'/d)-(2/3)(d'/d)+(1/3)(l^2/l'^2)(d'/d)}{1+(1/2)(l/l')(d'/d)-(1/2)(d'/d)}U^2. \quad \text{(B5)}$$

It is obvious that if d' is a small quantity compared with the thickness of the dielectric film and l/l' is always smaller than unity, the electrostatic energy per unit area is approximately equal to the value for the plane surface, i.e., equation (B5) is reduced to

$$E_e \approx \frac{\varepsilon\varepsilon_0}{2d}U^2. \quad \text{(B6)}$$